Seismic characterization of Cenomanian–Turonian carbonate platform based on sedimentological and geophysical investigation of onshore analogue outcrop (northern Lebanon)

Ghina Abbani, Mathilde Adelinet, Lama Inati, Cédric Bailly, Fadi Nader

Received: 4 April 2023 | Accepted: 22 June 2023

DOI: 10.1111/1365-2478.13396

Geophysical Prospecting | EAGE EUROPEAN ASSOCIATION OF GEOSCIENTISTS & ENGINEERS

ORIGINAL ARTICLE

Seismic characterization of Cenomanian–Turonian carbonate platform based on sedimentological and geophysical investigation of onshore analogue outcrop (northern Lebanon)

Ghina Abbani[1,3] | **Mathilde Adelinet**[2] | **Lama Inati**[3] | **Cédric Bailly**[4] | **Fadi Nader**[5]

[1]Sorbonne Université, ED398, Geophysics Laboratory, Paris Cedex 05, France

[2]IFP School, Georesources and Energy Center, Rueil-Malmaison, France

[3]CNRS-Lebanon, National Center for Geophysics, Dahr El Sawan, Lebanon

[4]Université Paris Saclay, CNRS, GEOPS, Orsay, France

[5]Geosciences Division, IFP Energies Nouvelles, Rueil-Malmaison Cedex, France

Correspondence
Ghina Abbani, Sorbonne Université, ED398, Geophysics Laboratory, BP 72-4, place Jussieu, 75252 Paris Cedex 05, France.
Email: ghina.abbani@cnrs.edu.lb

Funding information
CNRS-Lebanon and Campus France

Abstract

Outcrop analogues play a key role in the characterization of subsurface carbonate platforms. The lack of well data and relevant outcrop analogues can result in the misinterpretation of seismic data. To address this issue, we apply an integrated workflow based on sedimentology, geophysics and petrophysics on outcrop analogues present onshore Lebanon, to constrain the carbonate platform's properties on onshore seismic data. A thorough sedimentary description is completed for a 400-m-thick Cenomanian–Turonian carbonate platform located in Kfarhelda, northern Lebanon. P-wave velocity is acquired directly on the outcrop, and the petrophysical properties are measured on 44 samples. A 1D synthetic seismogram is computed with Ricker wavelet 25 Hz resembling seismic resolution. The resulting reflectors are mainly (1) high amplitude reflectors at the limit between two facies with contrasting physical properties enhanced by diagenesis, (2) moderate amplitude reflectors corresponding to stratigraphic limits at the transition between facies and (3) very low amplitude reflectors in karstified units. The integration of outcrop and seismic data is based on the generation of the synthetic seismogram to identify the geological origin of reflectors. The best fit between the synthetic seismic and seismic profile is used to interpret a seismic facies representing bedded limestones of Sannine and Maameltain formations (Cenomanian–Turonian). Two other distinctive reflectors are identified at the boundary of the Marly Limestone Zone, and the Channel facies unit characterized by bioclastic packstone to floatstone. This study highlights the importance of using outcrop analogues to identify the seismic signal of stratigraphic sequences and improve the interpretation of onshore seismic data.

KEYWORDS
acoustics, interpretation, reservoir geophysics, seismics, velocity analysis

INTRODUCTION

Seismic reflection is an essential method used to provide insights into sedimentary basin's architecture and tectonosedimentary evolution (Eberli et al., 2004). Seismic reflections result from the contrasts in acoustic impedance (AI), a product of sonic velocity and density (Sheriff, 1977). Even with little variation in composition and mineralogy, carbonates show a wide range of velocity and AI (Anselmetti & Eberli, 2001). Such changes are strongly related to the variation of porosity and pore structure, which is influenced by primary microstructures acquired during sediment deposition, as well

as secondary microstructures modified by diagenetic processes (Adelinet et al., 2019; Bailly, Adelinet, et al., 2019; Fournier & Borgomano, 2007).

The interpretation of seismic data is based on stratigraphic principles correlating genetically related sedimentary strata at depth (Vail et al., 1977). The reflectors are presumed to follow depositional surfaces and erosional unconformities (Mitchum, 1977). Seismic facies analysis was introduced as a useful tool to better interpret carbonate rocks on seismic data and provide a more complete geologic insight within a sedimentary basin (Berg, 1982; Fontaine et al., 1987; Mitchum, 1977). However, carbonates are greatly impacted by diagenetic processes that lead to spatial changes in porosity and pore structures, thus, altering the primary petrophysical properties of rocks (Teillet et al., 2020; Wagner, 1997). As a consequence, the seismic image may be disrupted, and the sedimentologic and stratigraphic interpretations of seismic data become more challenging (Anselmetti & Eberli, 2001; Eberli et al., 2003; Fournier & Borgomano, 2007). To understand the geological origin of seismic reflectors, the integration of sedimentologic and stratigraphic description with a physical characterization of rocks is essential.

Synthetic seismic modelling was presented as a primary tool to correlate seismic data with borehole data for better control of subsurface mapping (Embry et al., 2021; Rekoske & Hicks, 1992; Teillet et al., 2020). Two-dimensional synthetic seismic modelling is used to generate seismic sections for large-scale outcrop analogues and compare them to the subsurface seismic data. This method is based on ultrasonic measurements and petrophysical characterization of samples collected from outcrops (Jafarian et al., 2018; Kleipool et al., 2017; Zeller et al., 2015).

Nevertheless, a P-wave velocity measured at plug scale is not accurately representative of heterogeneities at the outcrop scale. For instance, Matonti et al. (2015) discussed the scale dependency of P-wave velocity in which in situ velocities are generally lower than plug-scale velocities because of large heterogeneities (diagenesis, fractures, stylolites). Bailly, Fortin et al. (2019) used a multiscale representative elementary volume concept to explain P-wave velocity variation due to upscaling. Although matrix porosity controls the ultrasonic P-wave velocity at the plug scale, crack and fracture porosity appears to impact significantly the sonic and seismic velocities, respectively. Therefore, with upscaling, P-wave velocity values vary in response to different geological heterogeneities (Boadu & Long, 1996; Lubbe & Worthington, 2006; Matonti et al., 2015).

In this study, we apply an integrated workflow based on the geological characterization of a Cenomanian–Turonian carbonate platform (onshore northern Lebanon) and its physical properties (acoustic, density, porosity) to generate a 1D synthetic seismogram. A thorough sedimentological description is completed for the studied outcrop located in Kfarhelda, north Lebanon (Figure 1a). Then, P-wave velocity is acquired directly at the outcrop, whereas porosity and density values are measured on representative samples in the laboratory. The constructed low frequency synthetic seismogram (25 Hz) is used to compare geological information from the outcrop with the onshore seismic data. This paper aims to (1) identify the relative control of facies distribution and lithological variations on the generation of seismic reflectors and (2) correlate outcrop data with onshore seismic data to identify the seismic signature of stratigraphic sequences.

GEOLOGICAL BACKGROUND

The Eastern Mediterranean is a collage of fragmented tectonic terranes situated among the African, Arabian and Anatolian plates (Figure 1a). The formation of the Eastern Mediterranean was induced by three main rifting phases during the Late Permian, Late Triassic and Early Jurassic. In the Late Jurassic, the rifting activity ceased and the initiation of passive margin was succeeded by the deposition of marine carbonates and deep-water siliciclastics along the westward-deepening slope (Dercourt et al., 1986; Gardosh et al., 2010; Garfunkel, 1998; Hawie et al., 2015; Robertson, 1998; Wood, 2015).

Onshore Lebanon, the Jurassic succession represents the core of Mount Lebanon deposited during prevailing shallow-marine carbonate platform settings. During the Late Jurassic, a global relative sea level fall and the following continental volcanism led to the deposition of Bhannes formation (Figure 1b; Abdel-Rahman, 2002; Walley, 1997). The uppermost Kimmeridgian–Tithonian is characterized by a shallow-marine platform representing Bikfaya and Salima formations, deposited in warm conditions, following a marine transgression (Walley, 1997). The Bikfaya formation is composed of massive fossiliferous carbonates with chert nodules (Nader et al., 2007), whereas the Salima formation represents a massive-to-thinly bedded oolitic limestones alternating with brown marls (Dubertret, 1975; Walley, 1997). The Late Jurassic–Early Cretaceous period was characterized by uplift and local emergence in northern Lebanon. As a result, the Jurassic–Cretaceous boundary is marked by an erosional unconformity in which the Berriasian rock units are absent from the Levant margin (Abdel-Rahman, 2002; Dubertret, 1975; Nader et al., 2007). Chouf formation overlies this unconformity representing fluvio–deltaic siliciclastic sediments (Walley, 1997). Overlying the Chouf formation is a transition unit of fossiliferous limestones, marls and sandstones known as Abeih formation (Late Barremian) (Dubertret, 1975).

Sea-level rises during the Aptian resulted in the deposition of massive (reefal) limestones known as the Mdairej formation (Walley, 1997). The overlying Hammana formation is composed of limestones, marls and terrigenous sediments

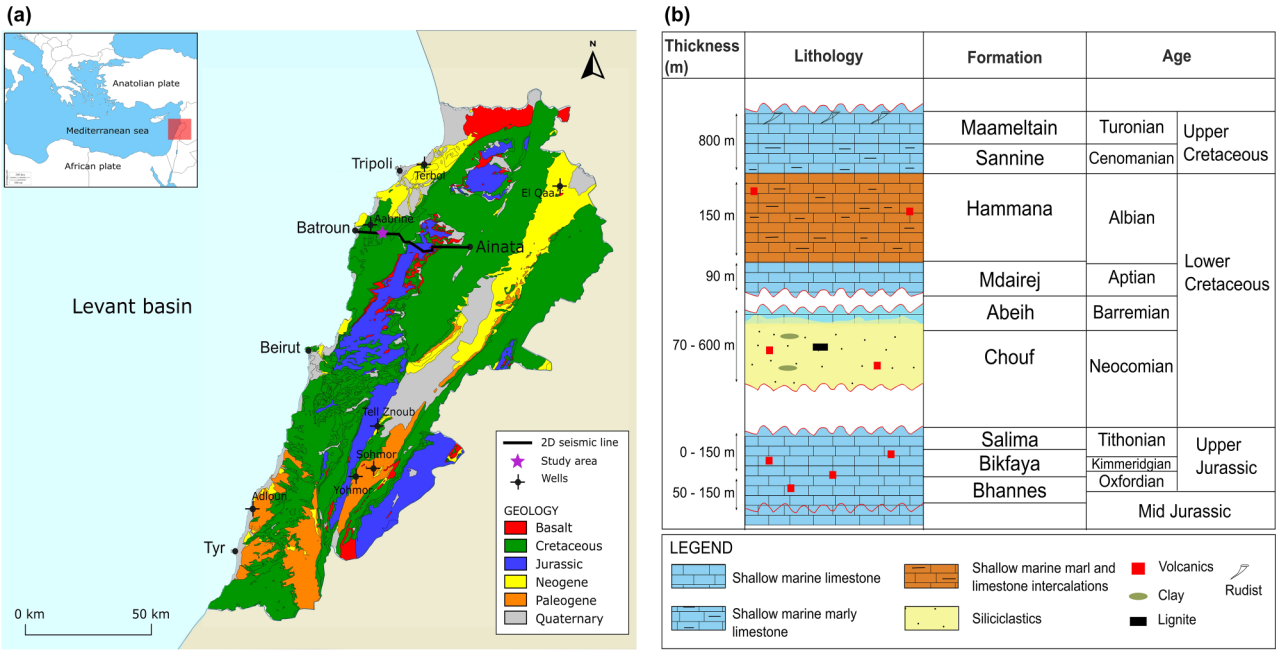

FIGURE 1 (a) Simplified geological map of Lebanon showing the trace of the onshore seismic profile, and the location of the study area and available onshore wells (edited after CNRS-Lebanon; Dubertret, 1955; Nader, 2011). (b) Simplified chronostratigraphic chart for onshore Lebanon showing the principal formations and sedimentary facies in north Lebanon from Upper Jurassic to Upper Cretaceous.

deposited in near-shore conditions during the Late Aptian to Albian (Noujaim, 1977). Maximum transgression prevailed in northern Lebanon from the Cenomanian and resulted in the deposition of Sannine formation which shows east–west facies change (Nader et al., 2016). Shallow-marine medium-to-thick-bedded limestones are observed to the east, whereas thinly bedded, chalky and cherty sediments are observed westward in deeper-marine conditions (Nader et al., 2006; Walley, 1997). Finally, shallowing-marine conditions prevailed during the Turonian leading to the deposition of Maameltain formation. It is composed of massive-to-thinly bedded limestone alternating with marls and representing a shallowing-upward trend, in which outer ramp facies are overlain by shallower marine facies, followed by a sharp return to deeper-marine conditions (Dubertret, 1975; Hawie, Deschamps, et al., 2013; Noujaim, 1977).

METHODOLOGY

The studied Kfarhelda outcrop represents a Cenomanian–Turonian succession of carbonates (Hawie, Deschamps, et al., 2013). The age of this sedimentary infill is well constrained by sedimentologic and biostratigraphic studies (Hawie, Deschamps, et al., 2013; Nader, 2000). Our study focuses on the upper part of Sannine formation composed of medium-to-thick bedded limestone, and the overlying Maameltain formation characterized by rudist-rich limestone.

Field work

Sedimentological investigation

A thorough sedimentary description was completed for the 400-m-thick Kfarhelda sedimentary section including lithology and texture description of each bed. Based on field observations and facies description, we defined facies associations (FAs) and built a sedimentary log.

Acoustic properties

P-wave velocity was acquired directly on the outcrop using Pundit PL-200 device, under atmospheric pressure and in dry conditions. The waves propagate through the rock between the transmitter and the receiver were the total travel time is recorded, and the velocity is obtained by dividing the total travel time to the spacing between the sensors, with less than 5% travel time error (Bailly, Fortin, et al., 2019). The velocities were obtained using 40 kHz P-wave sensors. The spacing (L) between the emitter and receiver is maintained constant at around 40 cm. This ensures that the number of cumulative wavelengths is enough to have a representative velocity data set. The measurements are acquired horizontally, parallel to the bedding, with a vertical spacing of 1 m. The inclination of the beds allowed us to measure the acoustic properties of 419-m-thick sedimentary series.

Laboratory measurements

A total of 44 samples were collected from the outcrop, relatively one sample every 10 m along a vertical section. Depending on their size, the samples were cut into cubes to acquire physical properties. The density and porosity values of rock samples were calculated using triple-weight method by measuring sample mass in dry condition, fluid-saturated condition and fluid-saturated submerged in the saturating fluid. First, the samples are dried in oven at 60˚C for 24 h to measure the dry mass (m_{dry}). Then, the samples are placed in a desiccator connected to a pump to ensure vacuum conditions for a minimum of 8 h. The desiccator is connected at the same time to an Erlenmeyer filled with de-mineralized water. The water is routed to the desiccator, and the samples are soaked for minimum 12 h. Finally, the submerged mass (m_{sub}) and saturated mass (m_{sat}) are measured, and the porosity, bulk density and mineral density are calculated based on the following equations:

$$\text{Porosity} = \frac{M_{sat} - M_{dry}}{M_{sat} - M_{sub}} \times 100, \quad (1)$$

$$\text{Bulkdensity}(\rho_{bulk}) = \frac{M_{dry}}{M_{sat} - M_{sub}}, \quad (2)$$

$$\text{Mineraldensity}(\rho_{min}) = \frac{M_{dry}}{M_{dry} - M_{sub}}. \quad (3)$$

Synthetic seismic modelling

Based on the outcrop and laboratory data set, a 1D synthetic seismogram is generated. The seismic response is primarily controlled by acoustic impedance (AI) representing the product of P-wave velocity (V_p) and bulk density (ρ_{bulk}). Two approaches were applied to calculate AI values while accounting to the resolution difference between velocity and density data. In the first approach, assumptions were made on density values to create grid dimensions comparable to the velocity grid. These assumptions were based on density values measured from the samples, and the sedimentological observations on the outcrop. In the second approach, AI values were calculated based on average velocity values comparable to the density grid dimensions. The two seismograms show good fit as a low frequency Ricker wavelet is used in generating the seismic trace.

The computed AI is used to calculate the reflection coefficient (RC) (Equation 4), which is then convoluted to seismic trace at zero-phase Ricker wavelet (Jafarian et al., 2018; Stafleu et al., 1994).

$$RC = \frac{AI_2 - AI_1}{AI_2 + AI_1}. \quad (4)$$

The Ricker wavelet is the second derivative of the Gaussian function, defined by one central frequency. It is widely used in synthetic seismic computation as its asymmetrical amplitude spectrum is similar to the attenuation feature of seismic wave propagation (Wang, 2015). In this study, a zero-phase Ricker wavelet was used to generate the seismogram as the 2D onshore seismic profile was processed using zero-phase conversion.

For P-wave velocity between 2000 and 6000 m/s, using a central frequency 25 Hz implies a resolution between 20 and 60 m (wavelength/4). This allows the comparison between the outcrop geological data and the onshore 2D seismic profile.

Seismic interpretation

The 2D seismic profile SLEB-2D-01-13 with EW orientation (Figure 1a) was acquired in 2013 and processed by Spectrum Geo Ltd. following Kirchhoff Pre-stack Time Migration (PSTM). PSTM was run with velocities smoothed over 2 km, 1 km and 500 m intervals when appropriate for the final pass of velocity analysis using CDP gathers, constant velocity stacks and contoured semblance displays. The line has a 44 km linear distance from Batroun coastal city to Ainata village passing through difficult irregular terrains. The interpretation of the profile was done at the Lebanese Petroleum Administration using Petrel software. Interpretation and time–depth conversion were completed after the work of Nader et al. (2016). The depth of time-picked reflectors was calculated using the proposed velocity model based on Dix equation (Dix, 1955; see Nader et al. (2016) for velocity model). Additionally, detailed sedimentological interpretation of Kfarhelda outcrop was used to identify local seismic facies of Cenomanian–Turonian age.

Seismic attributes represent the internal properties of a seismic signal obtained from seismic data (e.g. amplitude and frequency) (Nanda, 2016). It is considered a helpful tool for distinguishing lateral lithological changes (Chopra & Marfurt, 2007). The seismic attributes used in this study are the relative AI and the root mean square (RMS) amplitude. Relative AI attribute represents contrast in physical properties or apparent AI. It is used for lithology discrimination and variations in thickness. Additionally, it can indicate unconformity surfaces, discontinuities or sequences boundaries (Oyeyemi & Aizebeokhai, 2015). RMS attribute is also related to AI and is similar to reflection strength. Higher AI values imply higher RMS amplitude. It is also used to detect

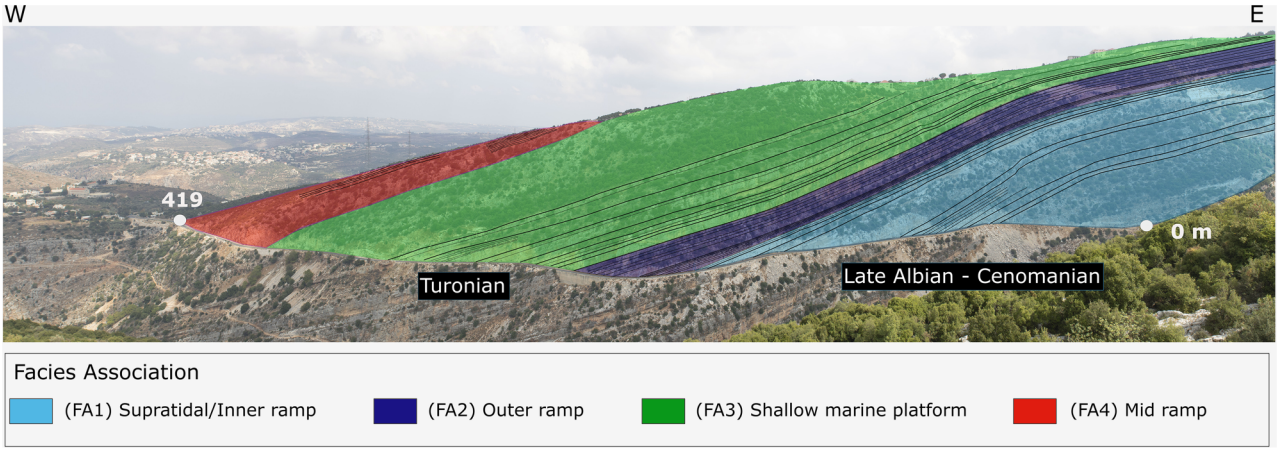

FIGURE 2 Panoramic view of the Kfarhelda outcrop, northern Lebanon, showing the identified facies associations. Black lines inside each facies association represent the bedding. Points 0 and 419 m represent the first and the last studied points, respectively.

unconformities, lithology changes and channels variations (Emujakporue & Enyenihi, 2020).

RESULTS

Sedimentary log description

Based on field and samples observations, 13 facies were identified for the entire stratigraphic interval, defining 4 facies associations (FAs): supratidal/inner ramp (FA1), outer ramp (FA2), shallow-marine platform (FA3) and mid-ramp (FA4) (Figure 2).

The lower 5 m of the section present fine crystalline dolomites dominantly laminated with calcite pseudo-morphs. These are overlain by a massive unit of bioclastic wackestone (Figure 3a), intercalated with thin layers of mudstone (1–3 m) up to 40 m. It is characterized by frequent calcite cemented vugs, weathering and fracturing, as well as porosity (micro- and fenestral porosity). Between 41 and 80 m, the texture becomes dominantly mudstone with cherts (Figure 3b). This mudstone unit is characterized by frequent stylolites (Figure 3c), bioturbations, fracturing and weathering.

A bioclastic-rich packstone to wackestone unit dominates the section between 82 and 129 m with mud intercalations, overlain by 6 m of bioclastic floatstone (131–137 m) (Figure 3d). Then, a unit of laminated mudstone with cherts is observed from 139 m with intervals of packstone (153–160 m), followed by another unit of mudstone up to 178 m. Between 179 and 213 m, the texture changes into massive bioclastic packstone to wackestone, with mudstone interbeds. It is followed by a unit of mudstone with internal erosion, and reworking breccias with slumping structures between 214 and 218 m (Figure 3e).

Between 219 and 267 m, we observed a unit of bioclastic-rich rudstone to grainstone with abundant rudists and gastropods (Figure 3f). This unit is also interbedded with bioclastic mudstone to wackestone layers (1–5 m). The outcrop was not describable from 285 to 294 m. At 300 m, we identified a layer of algal boundstone (Figure 3g), overlaid by a thick unit of dolomites (303–329 m) (Figure 3h). A thick unit of massive bioclastic wackestone to packstone is observed between 330 and 346 m, overlain by alternating units of dolomites and mudstone up to 382 m. It is followed by a massive, brecciated rock unit (2–5 m) at 383 m, alternating with layers of thinly bedded bioclastic rudstone to packstone (1–4 m) (Figure 3i) up to the top of the log at 419 m. These observations are used to build a sedimentary log of the outcrop representing Cenomanian–Turonian carbonate rocks (Figure 4).

Acoustic and petrophysical data set

P-wave velocity, density and porosity

A total of 419 P-wave velocity values were acquired at the outcrop. P-wave velocity shows high variability ranging between 1460 and 6400 m/s with a median of 4660 m/s. The distribution of acoustic properties according to the facies and FA classification is presented in a violin plot (Figure 5a,b). FA1 shows velocity values between 2800 and 5700 m/s, except for mudstone to wackestone facies (F1b) showing great variations between 1460 and 6100 m/s. FA2 presents generally higher velocity values between 3700 and 6000 m/s. Finally, FA3 and FA4 present velocity between 3200 and 6400 m/s, where the lower velocities (between 3600 and 4600 m/s) are associated with rudstone to grainstone facies (F3a).

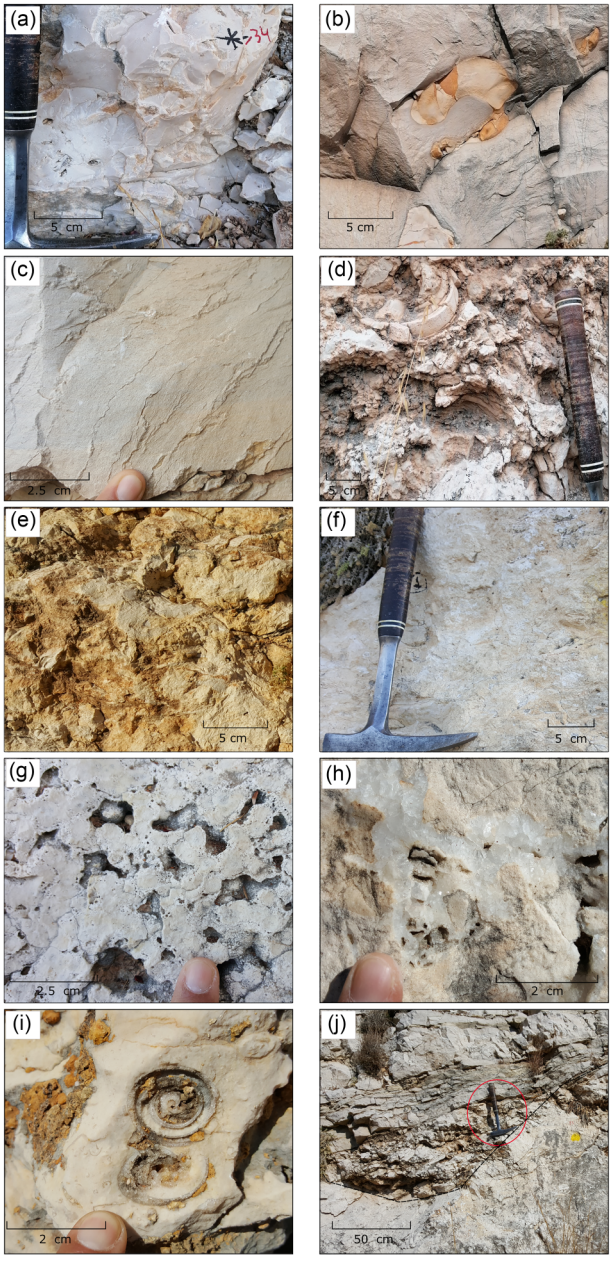

FIGURE 3 Cenomanian–Turonian facies of Kfarhelda outcrop: (a) bioclastic wackestone; (b) mudstone with chert nodules; (c) mudstone with stylolites; (d) bioclastic floatstone; (e) sedimentary breccia; (f) rudist-rich rudstone; (g) red algae boundstone; (h) dolomite with cemented vugs; (i) bioclastic rudstone; (j) channel facies.

The porosity and density values were calculated from 44 representative samples. Porosity varies between 1% and 17%, representing low-to-moderate porosity, with nine samples having porosity greater than 10%. Facies with muddy textures have generally lower porosity values (<5%), whereas bioclastic packstones to wackestone/floatstone facies (F1d and F3b) have an average porosity of 7.65%. Moderate porosity is observed for rudstone facies (~11%), and dolomite facies (F1a and F3d) have porosity values between 5% and 16%. Finally, bulk density varies between 2.23 and 2.67 g/cm^3, whereas mineral density varies between 2.56 and 2.8 g/cm^3. The plot between density and porosity shows decreasing density values with increasing porosity (Figure 5c). Most of the samples show values lower than the pure calcite and pure dolomite values. This can be explained by the depositional history and subsequent diagenetic processes impacting the primary petrophysical properties of rocks. For instance, fracturing and abundance of stylolites are observed between the base of the outcrop and around 190 m. FA3 facies are characterized by partial dolomitization associated with dissolution phases creating vugs, whereas FA4 facies are impacted by fracturing and brecciation. These diagenetic modifications can contribute to lowering the bulk density values.

Vertical evolution of physical properties and synthetic seismic

Figure 6 shows the vertical evolution of the geological properties of Kfarhelda outcrop compared to the measured physical properties: P-wave velocity, porosity, density and acoustic impedance (AI). P-wave velocity changes abruptly between the base of the log and 50 m. Between 40 and 48 m, mudstone to wackestone facies (F1b) is associated with the lowest velocity values (~1400 m/s). P-wave velocity values are centred between 3800 and 5800 m/s up to 100 m. This mud-supported facies (F1c) present porosity values between 1% and 8.7%. It is dominated by fractures and stylolites, which are intense between 54 and 82 m. Then, between 100 and 179 m, higher porosity values (~16%) are observed for bioclastic packstone to floatstone facies (F1d) and are associated with lower velocity values (3700–4600 m/s). From 180 to 218 m, FA2 is associated with low porosity and velocities centred between 3800 and 5000 m/s. Between 219 and 231 m, a unit of bioclastic rudstone to grainstone (F3a) is characterized by higher porosity (8%–16%), and velocities lower than 4600 m/s. The velocity is centred between 4000 and 5100 m/s up to 300 m, along with the sedimentary facies' alternation between F3b and F3c. Stylolites are common within F3c, whereas intense fracturing is observed up to 330 m. The porosity appears almost homogenous between 300 and 380 m (~4.8%–7%), whereas the P-wave velocity shows a scattered pattern. Finally, at the top of the sedimentary log, F4a and F4c present velocity values between 3200 and 6000 m/s, whereas F4b (bioclastic rudstone to floatstone) present velocities centred between 5100 and 5900 m/s.

Along the previously described sedimentary log, the AI shows a vertical trend similar to that of P-wave velocity. AI is then used to calculate the reflection coefficient and generate a 1D synthetic seismogram representing the studied outcrop. Negative amplitude reflectors are in blue and correspond to

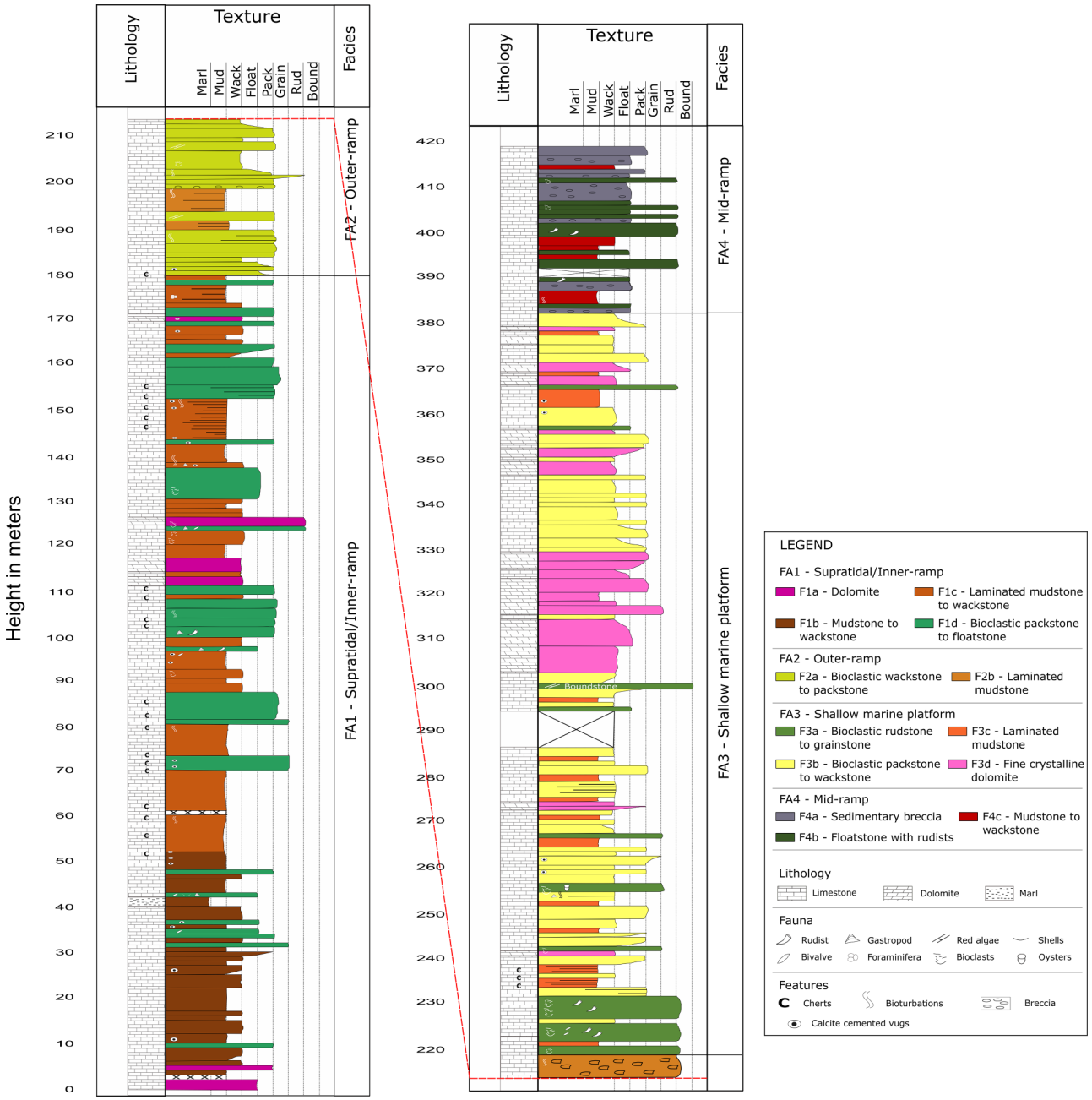

FIGURE 4 Simplified sedimentological log of Kfarhelda outcrop for Cenomanian–Turonian carbonate platform representing supratidal/inner ramp, outer ramp, shallow-marine platform and mid-ramp facies associations.

downward decrease in AI, whereas positive amplitude reflectors are in red and correspond to downward increase in AI. Six negative amplitudes (R1, R3, R5, R7, R9, R11) and six positive amplitudes (R2, R4, R6, R8, R10, R12) reflectors are identified. Reflectors R1, R2 and R3 appear to have higher amplitude than other reflectors. No reflections are observed on the seismogram between 115 and 145 m. Similarly, the reflectors observed between 340 and 385 m show very low amplitude.

2D Seismic profile

A detailed seismic stratigraphic analysis was completed on the seismic profile to identify the main reflectors near Kfarhelda outcrop. Six reflectors were identified on the cropped section of the profile: H1, H15, H14, H13, H10, H6 (Figure 7). Seismic facies analysis was carried out locally for the Upper Cretaceous interval to associate the prevailing reflection patterns with their relative depositional settings. For the

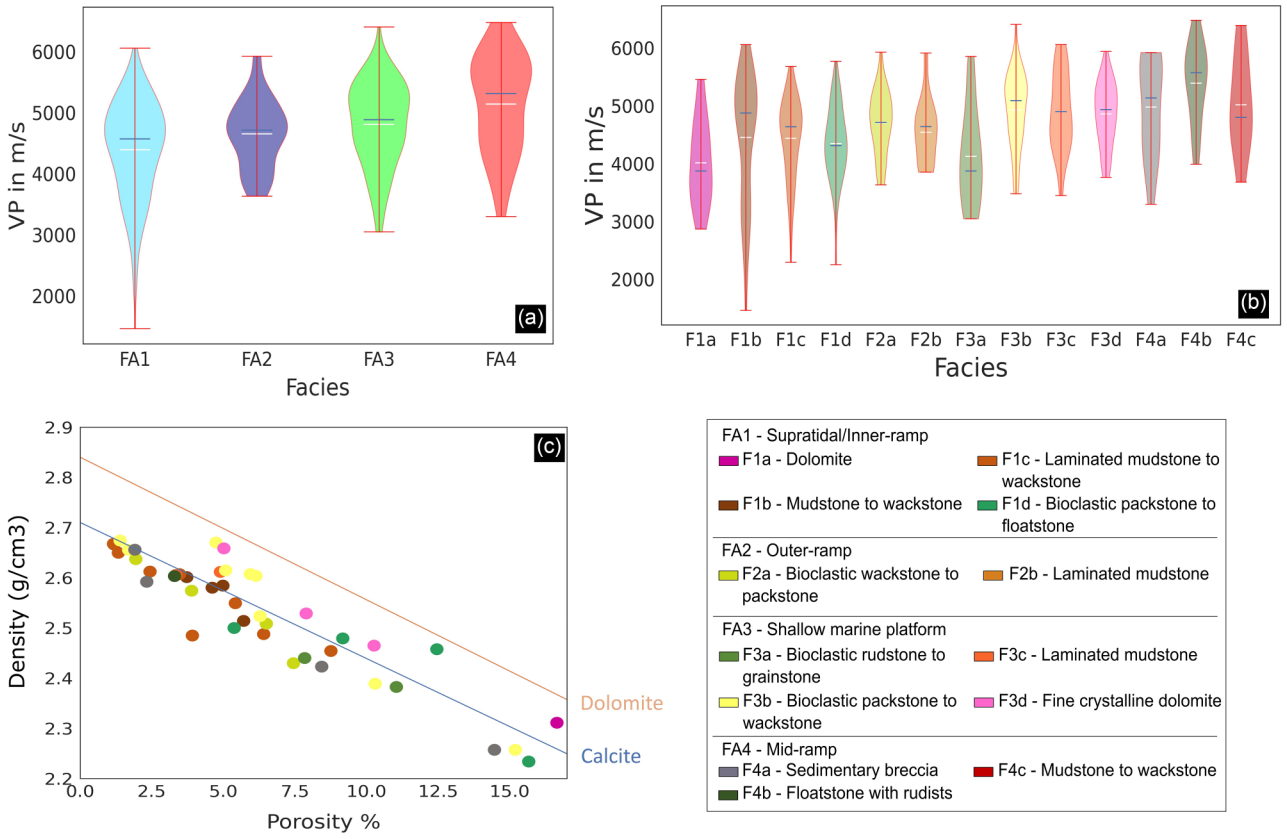

FIGURE 5 (a) Violin plot showing the distribution of P-wave velocities over facies associations, (b) violin plot showing the distribution of P-wave velocities over different facies (the mean is presented as black horizontal dash, and the median is presented as green horizontal dash), (c) density versus porosity acquired from 42 rock samples, and the legend identifying the included facies.

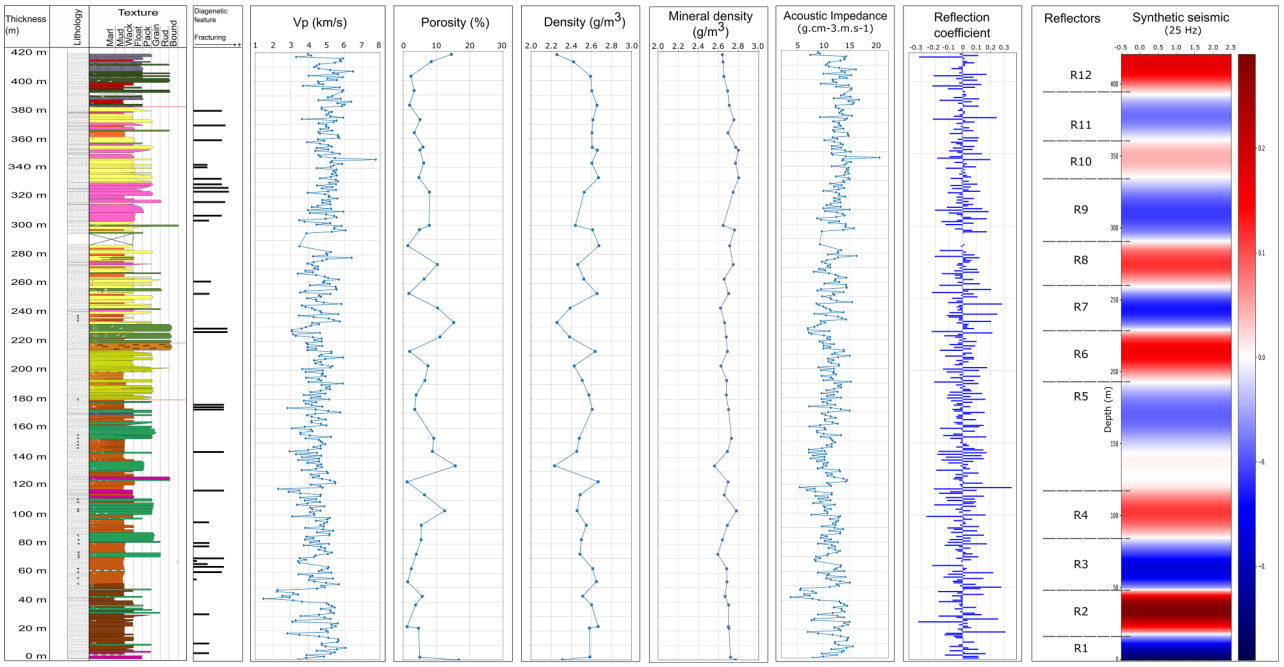

FIGURE 6 High resolution seismic stratigraphy showing a simplified sedimentary log and the relative fracturing intensity; velocity values at outcrop scale (m/s); porosity (%), mineral and bulk density (g/cm^3) acquired on samples; acoustic impedance (g/cm^3, m/s); reflection coefficient; synthetic seismogram and the identified seismic reflectors.

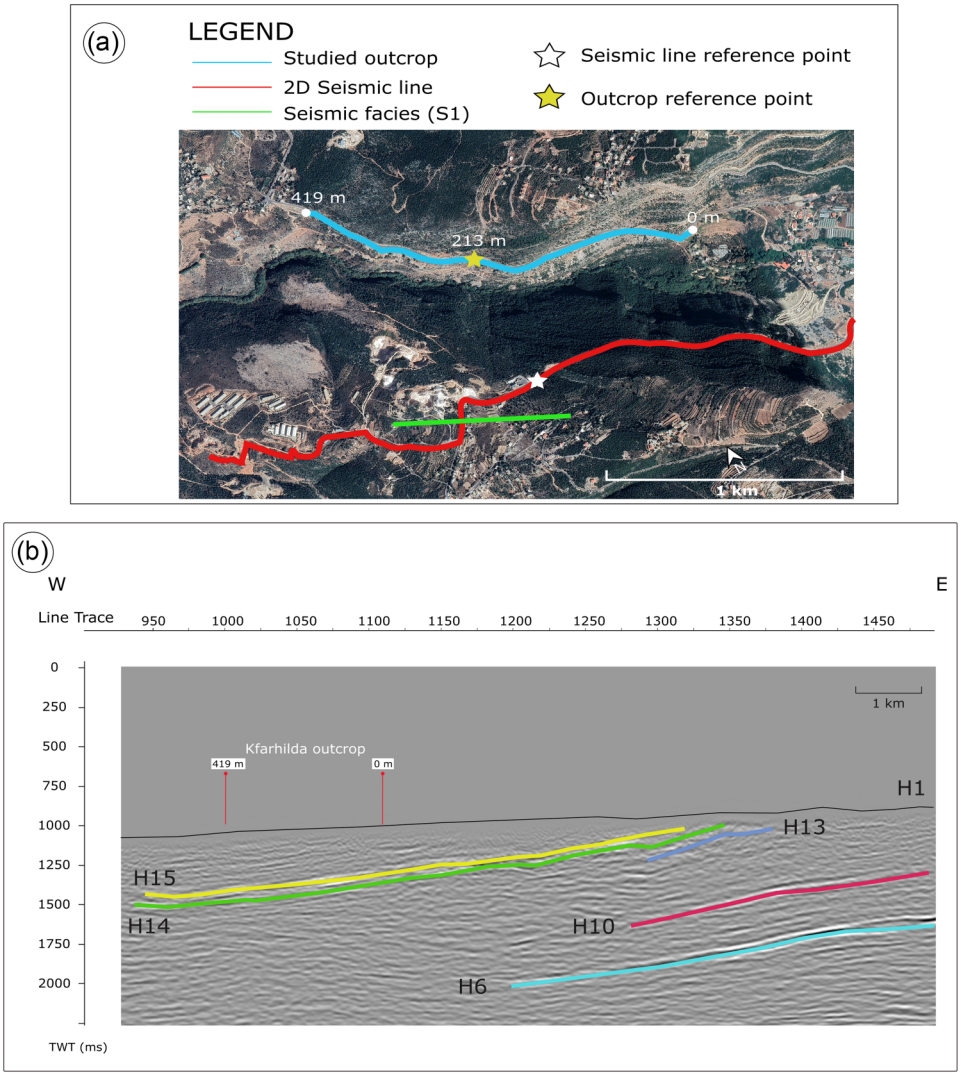

FIGURE 7 (a) Satellite image of Kfarhelda area showing the locations of seismic line trace, studied outcrop and the relative location of seismic facies S1; (b) cropped image from central part of the interpreted seismic profile SLEB-2D-01-13 showing the key reflectors near the Kfarhelda outcrop, and the location of the studied outcrop.

Cenomanian–Turonian deposits in Kfarhelda area, four main types of seismic facies (S1, S1, S3, S4) are classified based on reflection characteristics.

DISCUSSION

Sedimentary facies associations

The completed fieldwork provided a sedimentary log covering of the Cenomanian–Turonian outcrop studied in Kfarhelda. Four facies associations (FAs) were identified for the outcrop based on field observations and literature of regional geology and stratigraphic evolution of northern Lebanon (Beydoun, 1977; Dubertret, 1975; Hawie, Gorini, et al., 2013; Nader, 2011; Saint-Marc, 1972). The Cenomanian–Turonian carbonate platform prevailed along the Levant margin and presented important rudist accumulations along the Turonian mid-ramp configuration (Nader, 2000; Saint-Marc, 1972). The FAs attested in Kfarhelda outcrop fit well with major eustatic fluctuations during the Cenomanian–Turonian.

The FA (FA1) at the base of the outcrop refers to supratidal/inner ramp configuration. Laminated fine crystalline dolomite (F1a) represents the supratidal depositional setting. F1b consists of massive thinly bedded mudstone to wackestone, and F1c represents a unit of thinly bedded mudstone to wackestone with cemented vugs. The main difference with F1c is the abundance of chert nodules marking deepening conditions, consistent with the maximum transgression conditions affecting the Arabian plate from the Early Cenomanian to the Early Turonian (Sharland et al., 2001). F1d consists

of bioclastic-rich packstone to floatstone units with rudists, gastropods and bivalves, representing shallowing-upward channel facies (Nader et al., 2006).

Two facies are identified for the outer ramp FA (FA2): massive-to-thinly bedded bioclastic packstone to wackestone (F2a), and thinly bedded mudstone (F2b). Additionally, FA (FA3) represents shallow-marine platform consisting of bioclastic rudstone to grainstone facies with abundant rudists (F3a), and bioclastic packstone to wackestone facies (F3b). The Turonian carbonate platforms with rudist accumulations have been extensively studied on the Arabian Plate (Saint-Marc, 1972, 1974). During the Mid-Turonian, shallowing trend with major regression, enhanced by Levant marginal uplift, affected the Levant area explaining the sharp transition into the rudist-rich rudstone platforms (Haq et al., 1988; Hawie, Deschamps, et al., 2013). The dolomite textures with chicken wire structures (F3d) mark further shallowing and a shift into supratidal depositional setting (Nader et al., 2016).

The facies F4a (in FA4) consists of massive brecciated packstone indicating slope instability during the Mid-to-Late Turonian. The alteration of brecciated rock units could be due to the tectonic movements associated with the complex structural evolution of the Levant margin, such as the Syrian arc folding initiated from Late Turonian (Brew et al., 2001; Walley, 1998). Rudstone to floatstone facies (F4b) marks a progressive return to shallow-marine settings, followed by deeper laminated mudstone to wackestone facies (F4c) at the top of the Turonian series (Noujaim, 1977). The Levant margin is characterized by deepening of sedimentary facies during the Late Turonian (Hawie, Deschamps, et al., 2013).

Geological origin of seismic reflectors

Based on our data set and the synthetic seismic computation, the geological origin of seismic reflectors has been determined. Seismic reflections can be classified in three groups: (1) high amplitude reflectors resulting from vertical variation in petrophysical properties enhanced by diagenetic features (R1, R2, R3), (2) high-to-moderate amplitude reflectors resulting from a vertical change in acoustic impedance (AI) at the boundary between two facies or FA (R4, R5, R6, R7 and R12) and (3) low amplitude reflectors within karstified and fractured units (R9, R10, R11).

Reflector R1 (Figure 6) is a high amplitude negative reflector at the base of the log resulting from upward decrease in porosity at the transition between fractured dolomite (F1a) and tight mudstone facies (F1b). R2 is a high amplitude positive reflector controlled by positive reflection coefficients (RCs), whereas R3 is a negative reflector resulting from sharp contrast in AI at the transition between mud-dominated facies F1b and F1c. Both facies represent mud-supported limestone yet with two distinctive differences: F1b includes marl intercalations causing the sharp decrease in velocity values. In contrast, F1c represents mudstone with chert nodules and abundant stylolites. Consequently, velocity values observed for F1b and F1c show significant scattering (Figure 5b), outlining an impact of the outcropping diagenetic features. This implies that these high amplitude reflectors observed at the base of the log correspond to vertical facies variation and contrasts in physical properties enhanced by diagenetic features.

High-to-moderate amplitude reflectors form at the transition between two facies. For instance, a bioclastic packstone unit (F1d) is observed at 80 m representing a channel facies with coarsening upward trend. This unit is associated with lower velocity values and moderate porosity (~12%). The contrast with the underlying less porous mudstone units (F1c) resulted in the generation of the positive reflector R4. Conversely, R5 is a negative reflector representing a trend of decreasing upward porosity. Observations at the outcrop show an interesting contrast at around 150 m. This limit marks the end of bioturbation dominating the previous unit, and a fining upward trend.

Between 190 and 230 m, the log is dominated by bioclastic packstone (F2a) and rudstone to grainstone facies (F3a). This section is generally characterized by lower velocity values and increasing porosity (11%). Consequently, the sharp contrast with the underlying mudstone unit generates the positive reflector R6. This reflector represents an important stratigraphic limit, at the transition between FA2 and FA3, marking the Mid-Turonian shallowing trend and the deposition of rudist-rich rudstone platforms.

A unit of less porous bioclastic packstone (F3b) overlies the rudstone platform at around 233 m, generating the negative reflector R7. Conversely, the reflector R8 does not appear to represent a boundary or facies transition, but rather a vertical variation in porosity and AI pointing to a diagenetic contrast. Finally, R12 is a positive reflector marking the transition between FA3 and FA4, associated with an increasing porosity trend for the brecciated packstone unit (14%). This clearly demonstrates that the vertical variation in acoustic properties is related to facies variation in which the main reflectors remain in accordance with the depositional timeline and initial petrophysical properties.

The very low amplitude reflectors (R9, R10 and R11) at the upper part of the log are associated with a thick unit of dolomites (~30 m) and an overlying highly karstified section of alternating dolomite and mudstone/wackestone textures (mineral density ~2.8 g/m^3). The velocity values vary within these beds, whereas the porosity remains relatively low (4%–7%). This can be explained by the homogenization effect of diagenesis that masks the contrasts related to the vertical variation of facies (Bailly et al., 2022). Finally, sections that are characterized by vast variations of physical properties result

in rapid succession of beds with high AI contrasts. Consequently, the seismic signal is obliterated, and no reflectors are observed between 120 and 150 m.

Seismic interpretation and seismic facies analysis

Interpretation

A section of the onshore 2D seismic profile was interpreted to identify major seismic reflectors and assign proper lithostratigraphic attributes to the seismic facies. Figure 7a presents a satellite image showing the relative locations of the outcrop and the 2D seismic profile. Figure 7b shows the relative location of the studied Kfarhelda outcrop to the interpreted section of the 2D seismic profile.

Six reflectors were identified on the studied section of the 2D seismic profile (H1, H15, H14, H13, H10, H6) (Figure 7b). H1 represents the ground horizon and shows an increase in altitude eastwards with minor elevation near the study area. H15 is a continuous reflector with strong impedance present in the western part of the profile. It corresponds to the base of Albian–Cenomanian limestone of Hammana formation. The reflector H14 is also continuous with high impedance contrast that runs parallel to H15 just below Kfarhelda outcrop where it forms a mound-like feature dipping to the west. H14 limits the boundary between overlying parallel to sub-parallel continuous seismic package and the underlying sub-parallel, less continuous reflectors of high amplitude. The H15–H14 interval has an average thickness of 230 m which coincides with the thickness of Abeih and Mdairej Formations (Figure 1b).

H13 is a discontinuous reflector that underlies H14 at some places in the middle of the profile, whereas it forms a thin seismic package in the eastern part of the profile, characterized by continuous high amplitude reflectors. The thickness of this unit may be correlated with Chouf formation. H10 and H6 are strong non-continuous reflectors that extend from the centre of the profile eastward, with high impedance contrast. H10 underlies a thick seismic package in the east, below Mount Lebanon, whereas it shows elevation and discontinuity towards the centre. It then thins westward and becomes parallel to H13. H10 corresponds to Kesrouane formation (marly deposits) with average thickness H13–H10 between 810 and 1190 m in the west and thickens eastward. Finally, H6 is more continuous in the central and western parts of the profile marking the base of a similar seismic package. The interval H10–H6 has a thickness between 870 and 1300 m, thickening eastward. It corresponds to Early–Mid Triassic evaporites (Kurrachine anhydrites) considering that the Liassic and Triassic sequences have a total average thickness 1245 m (Nader et al., 2016).

Seismic facies analysis–cropped section near Kfarhelda

The proposed classification of seismic facies is based on reflection configuration, amplitude characteristics and the continuity of seismic reflectors (Figure 8). The seismic facies type S1 represents continuous parallel reflections with moderate amplitude. The analysis of amplitude suggests a unit of stratified deposits with significant lithological contrast. This can be explained by the presence of limestone layers (high-impedance) intercalated with marls (lower impedance) or marl-limestone alternations within thin beds (Słonka & Krzywiec, 2020). Such a unit can be related to the Upper Cenomanian unit of Sannine formation characterized by bedded limestones with chert intervals (Nader, 2014; Walley, 1997). S2 seismic facies type represents semi-continuous wavy parallel reflections with moderate-to-high amplitude. This type is identified at more than 300 m and the impedance contrast suggests that this unit is related to the massive, bedded limestones (with cherts) of Middle Cenomanian unit of Sannine formation (Nader, 2014; Walley, 1997). The type S3 seismic facies represents a mound-shaped semi-continuous to discontinuous reflection geometry with moderate amplitude. This lack of continuity is related to carbonate deposits forming reef bodies in a high-energy system (Veeken & Moerkerken, 2013). S3 is identified at 550–640 m which can be related to the reef limestones of Lower Cenomanian unit of Sannine formation.

Finally, seismic facies type S4 overlies the reflector H15 marking the base of Sannine formations at around 650 m depth. S4 represents chaotic and low amplitude seismic reflectors that could be linked to deposits with karst features related to Early Cenomanian massive dolomitic rocks defined as the Hammana–Sannine transition unit. Karst features have been interpreted in terms of seismic facies as chaotic seismic reflections with low amplitude (Burberry et al., 2016; Embry et al., 2021; Hendry et al., 2021; Hu et al., 2023; Sayago et al., 2012). This can be related to the petrophysical properties of karstified rocks often characterized by lower AI values compared to the surrounding rock units (Fournillon et al., 2021).

In Kfarhelda outcrop, seismic facies type S1 is dipping westward. It reaches down to 1.15 s (Figure 9a). The interpretation of surface geology, as well as the reflection characteristics, confirms that S1 was observed in other locations to the west of the seismic profile where the Turonian Maameltain formation outcrops.

Outcrop to seismic tie and seismic-stratigraphic context

P-wave velocities were acquired horizontally on the outcrop at 40 kHz frequency representing a pluri-centimetre

Seismic facies	Example - +	Characteristics	Depositional environment
S1 *Parallel - bedded*	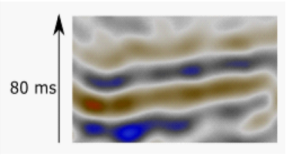	Parallel Continuous Moderate/low amplitude High frequency	Thinly bedded limestone Inner ramp
S2 *Parallel - bedded*	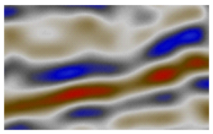	Parallel Semi-continuous Moderate amplitude High frequency	Massive bedded limestone Ramp
S3 *Mound - shaped*	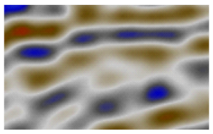	Mound-shaped Semi- to discontinuous Moderate amplitude Low frequency	Carbonate/ reef build-ups
S4 *Chaotic*	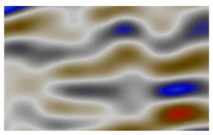	Chaotic Low amplitude Low frequency	Karst?

FIGURE 8 Results of seismic facies analysis of the Cenomanian–Turonian interval.

scale (40 cm). Acoustic measurements from Kfarhelda outcrop were acquired in dry conditions and under atmospheric pressure (0.1 MPa). In burial conditions, P-wave velocity is modified under the impact of confining pressure, depending on the condition of initial porosity, pore type and cracks (Anselmetti et al., 1997; Fournier et al., 2011; Matonti et al., 2015). The studied Cenomanian–Turonian carbonate outcrop shows a low amount of burial. Thus, the acoustic measurements acquired on the outcrop can be used to interpret the corresponding onshore seismic line.

The best fit between the synthetic seismic and seismic profile is presented in Figure 10. At the base of the sedimentary log, reflectors R1, R2 and R3 have the highest amplitude for synthetic traces at the vicinity of high RCs (in absolute value). Similarly, the seismic profile shows moderate amplitudes within seismic facies S1, particularly for reflectors S1b, S1c and S1d, whereas S1a shows lower amplitude (Figures 9a and 10). To correlate the outcrop data with seismic data, we introduce a pseudo well W1 representing the sedimentologic log of Kfarhelda outcrop (Figure 9a). The location was estimated based on the seismic trace and GPS data of the outcrop. The well represents the studied sedimentologic log between 0 and 213 m. The well reaches the Upper Cenomanian unit of 'Sannine formation' with a total thickness of 213 m. This unit is identified as the seismic facies S1 characterized by medium-to-thick bedded limestone and marly limestone sediments (Walley, 1998). The relative locations of W1 on the seismic line as well as the studied outcrop are shown in Figure 9a.

A succession comprised alternations of marl, marly limestone and mudstone is identified as the Marly Limestone Zone (MLZ), responsible for creating AI contrast. However, these marl intercalations have a relatively low thickness (~8 m), at the limit of resolution of seismic data. This results in seismic signal interference and seismic tuning due to the strong overlap of reflective signals from marl and limestone strata, making it difficult to precisely detect the limits of the marly zone using seismic data alone (Słonka & Krzywiec, 2020). Above the MLZ, a unit associated with inner ramp carbonate deposits is present and characterized by mudstone containing chert. Similarly, a unit of massive limestone (mudstone to wackestone) is present below MLZ and characterized by higher velocities. Consequently, the strong AI created at the limits of the MLZ results in a series of high amplitude (positive and negative) seismic reflectors.

The positive seismic reflector generated below S1d has a very low frequency and cannot be clearly interpreted. This can be related to the presence of the dolomite unit identified at the base of the well. This unit may extend deeper below the studied outcrop, resulting in a thick dolomite unit that can mask

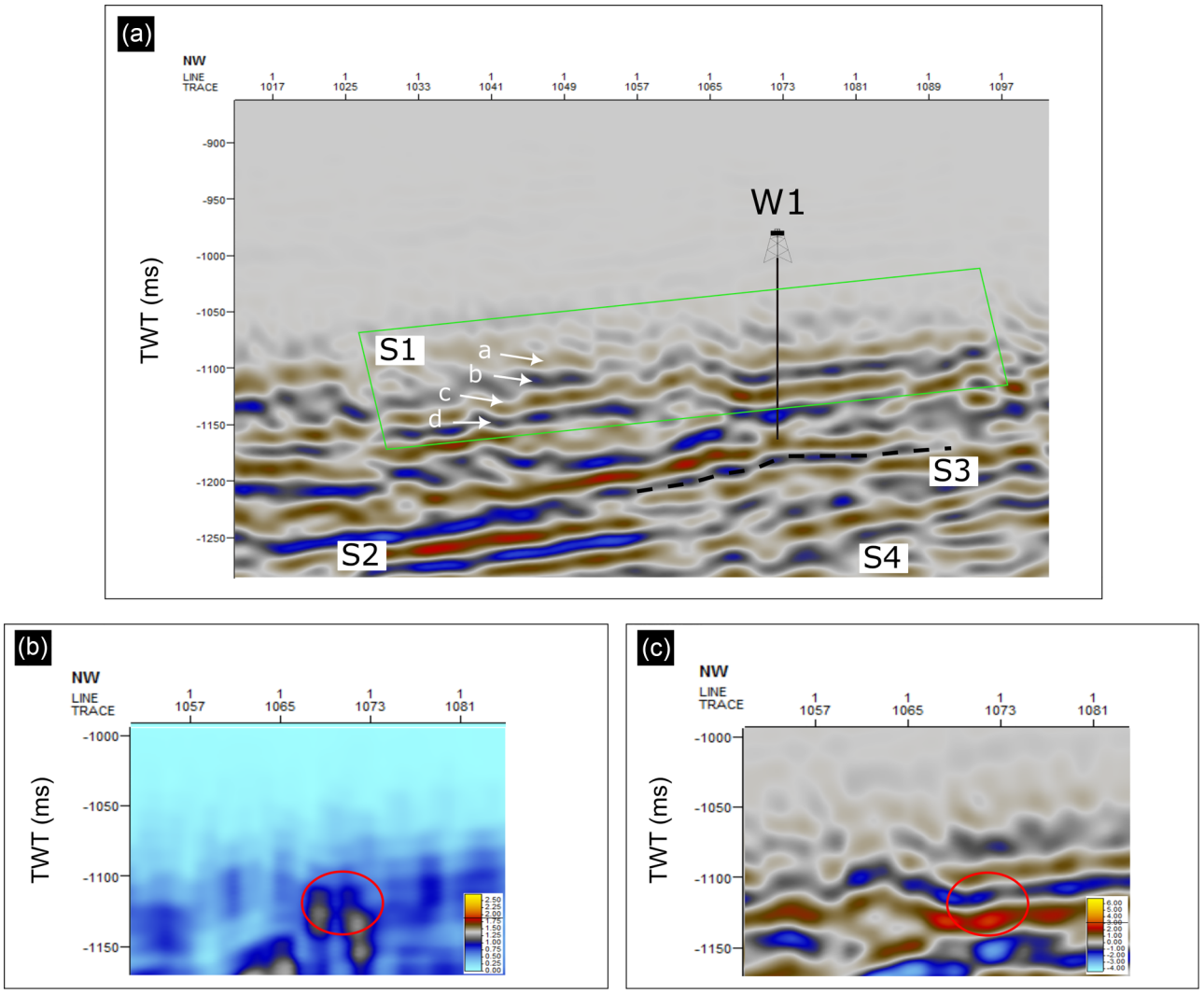

FIGURE 9 (a) Cropped image of the seismic profile, near the studied Kfarhelda outcrop, showing seismic facies and well W1 locations; (b) a cropped image of root mean square (RMS) amplitude and (c) relative acoustic impedance seismic attributes, applied on a section of the profile (Figure 10a), showing channel facies (circled).

the vertical contrast in AI. Consequently, a chaotic, low amplitude, low frequency seismic image is observed (Figure 9a). In contrast, the synthetic seismic reflectors R1 and R2 show higher amplitude because the vertical variation of physical properties is better represented on the synthetic seismogram, resulting in sharp contrasts and higher resolution reflectors.

A unit of channel facies is identified above the mudstone and characterized by coarsening upward trend. This unit, dominated by bioclastic floatstone, is associated with changes in physical properties (higher porosity and lower velocity). It induces a contrast in AI and, consequently, generates a seismic reflector (S1c). It corresponds to the reflector R4 on the synthetic seismogram, a positive reflector with moderate amplitude. Root mean square (RMS) and relative AI seismic attributes are used to distinguish channels for this section. Figure 9b,c shows that the channel facies unit identified on the sedimentologic log have a good match with the bright spots identified on the RMS seismic attribute. RMS attribute is usually used to detect bright spots of porous sand representing possible hydrocarbon reservoir (Brown, 2001; Mangal et al., 2004; McQuillin et al., 1984). Indeed, using RMS attribute to detect coarser-grained facies, such as channel facies, is an approach commonly used in the literature (Emujakporue & Enyenihi, 2020; Ghoneimi et al., 2021; Hossain, 2020; Oyeyemi & Aizebeokhai, 2015).

The stratigraphic and sedimentologic descriptions show that the seismic reflector S1b can be associated with a sharp transition between inner ramp deposits and a unit of supratidal dolomites. On the contrary, no reflectors are identified for the synthetic seismogram within this section. This was previously explained as signal cancellation resulting from rapid alternations in AI. At the top of the well, the synthetic seismic does not show a good fit with the seismic profile. Onshore seismic reflection data are generally characterized with

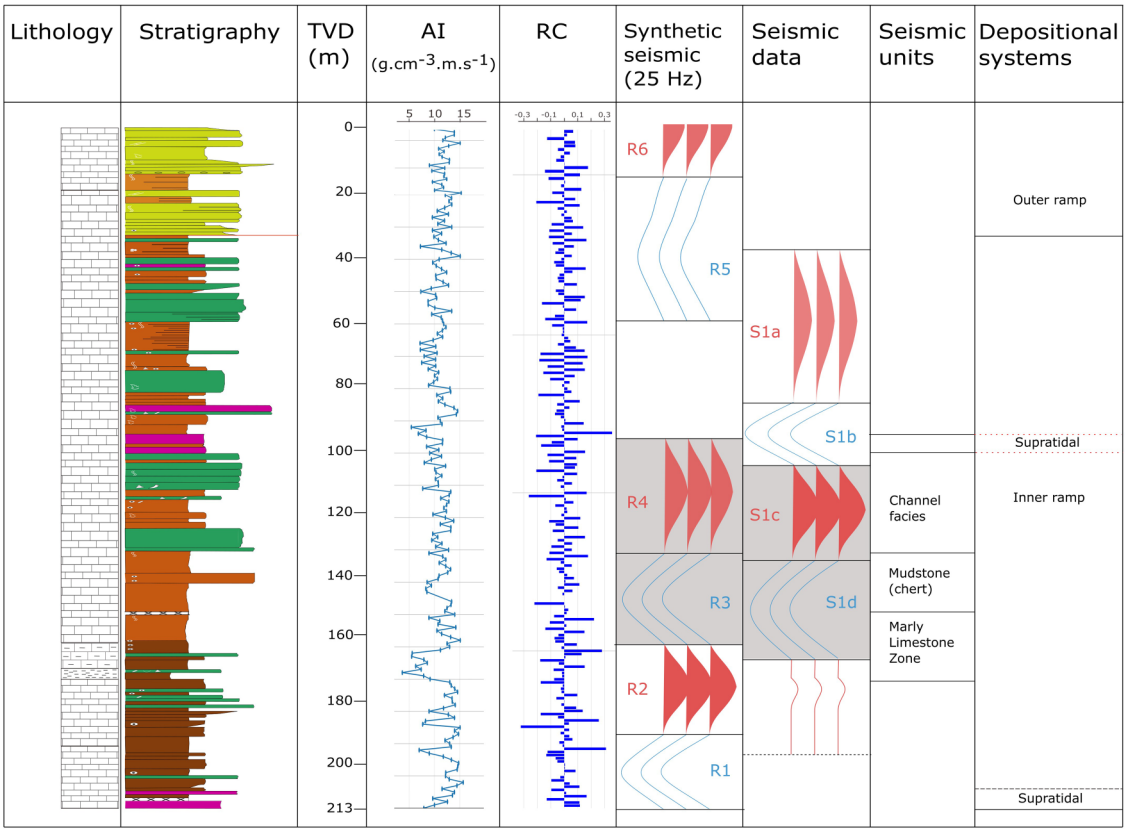

FIGURE 10 Results of well-to-seismic tie using synthetic seismogram, correlated with simplified sedimentological log for the Cenomanian–Turonian succession studied at Kfarhelda (purple for F1a, dark brown for F1b, light brown for F1c, dark green for F1d and light green for F2a). Synthetic seismic and seismic traces are represented in depth (m). Negative amplitude reflectors are presented in blue, and positive amplitude reflectors are in red. The main seismo-stratigraphic units: (1) channel facies and (2) Marly Limestone Zone are both related to Upper Cenomanian Inner ramp depositional setting.

seismic noise near the surface of the earth. The top 10–30 m are associated with slower velocities causing the wavelength to be shorter. Consequently, the wavelength is impacted by small-scale heterogeneities (0.5–10 m) causing energy scattering and distortion of the signal (Stork, 2020).

In summary, the major seismic reflectors are related to vertical variations of the principal physical properties, including porosity, mineralogy and velocity. The correlation between synthetic seismogram and seismic data generated for Kfarhelda outcrop shows two units with significant seismic signatures: the MLZ (high amplitude negative reflector) and channel facies (high-to-moderate amplitude positive reflector). This study provides a sedimentological characterization of the Cenomanian–Turonian sedimentary succession in north Lebanon. The interpretation of seismic data is often complicated by uncertainties and poor image quality. Indeed, outcrop analogues can provide a key tool for the characterization of a carbonate platform system by unravelling the geological details beneath the seismic reflection resolution (Hendry et al., 2021; Howell et al., 2014). The comparison between synthetic seismic models, based on observations and data from the outcrop, can provide insight into the best interpretation of the seismic data. In this study, the geological origin of seismic reflectors and the relative control of facies distribution were identified. These findings are of importance for the seismic interpretation of onshore profiles because it shows the seismic signature of the Cenomanian–Turonian stratigraphic sequence, making it an adaptable approach for similar sedimentary succession. Indeed, carbonate platforms exhibit a high degree of heterogeneity and reservoir complexity (Hendry et al., 2021). Our work demonstrates that the main seismic reflectors observed for the studied outcrop coincide with stratigraphic boundaries. However, this study highlights the need for advanced petrographic and petrophysical investigation to understand the intensity of diagenetic processes and their impact on the evolution of rocks' physical properties.

CONCLUSION

In the present study, we discussed the sedimentological and geophysical characteristics of a Cenomanian–Turonian shallow-marine carbonate platform located in Kfarhelda,

northern Lebanon. An extensive sedimentological investigation over the outcrop allowed the identification of four facies associations (FAs): supratidal/inner ramp (FA1), outer ramp (FA2), shallow-marine platform (FA3) and mid-ramp (FA4). Acoustic properties were acquired directly on the outcrop using Pundit PL (200) device. P-wave velocity values were obtained horizontally at 40 kHz frequency with 1 m vertical spacing. The integration of sedimentologic and acoustic properties from outcrop investigation with the petrophysical characterization of samples enabled the generation of a 1D synthetic seismogram convoluted using Ricker wavelet 25 Hz providing a seismic scale resolution.

The identified seismic reflectors belong to three groups: (1) high amplitude reflectors resulting from vertical variation in petrophysical properties enhanced by diagenetic features, (2) high-to-moderate amplitude reflectors resulting from a vertical change in acoustic impedance (AI) at the boundary between two facies or FA and (3) low amplitude reflectors corresponding to a highly karstified unit representing homogenized physical properties. The interpretation of the 2D seismic profile, near Kfarhelda outcrop, resulted in better understanding of the subsurface geology. Four seismic facies were identified corresponding to the Early Cenomanian–Turonian Sannine and Maameltain formations. The integration of outcrop and seismic data was done based on synthetic seismogram. The best fit between the synthetic seismogram and the seismic profile resulted in the following conclusions: (1) seismic facies S1 represents the Upper Cenomanian unit of Sannine formation characterized by medium-to-thick bedded limestones with marl intercalations and chert intervals, (2) the main seismic reflectors investigated within S1 are related to the Marly Limestone Zone causing sharp contrast in AI, and the overlying channel facies characterized by bioclastic packstone–floatstone with higher porosity, and (3) near surface reflectors are impacted by noise causing signal distortion. Thus, assessing the geological origin responsible for the reflection and the true thickness of rock unit is less accurate.

Finally, applying this approach on similar outcrops will aid in investigating the complete Cenomanian–Turonian carbonate platform, for better petrophysical and acoustic characterization of facies and constraining of the carbonate platform properties on seismic data.

ACKNOWLEDGEMENTS

This work is part of the PhD project of the first author, a collaboration between CNRS-Lebanon, Sorbonne University, and IFP Energies Nouvelles. The work is financially supported by CNRS-Lebanon and Campus France. We thank the Lebanese Petroleum Administration (LPA) for providing seismic data and access to Petrel software.

DATA AVAILABILITY STATEMENT

The data set used in this paper is available from the corresponding author (GA).

ORCID

Ghina Abbani https://orcid.org/0009-0000-8734-9544

REFERENCES

Abdel-Rahman, A.M. (2002) Mesozoic volcanism in the Middle East: geochemical, isotopic and petro-genetic evolution of extension-related alkali basalts from central Lebanon. *Geological Magazine*, 139(6), 621–640.

Adelinet, M., Barthélémy, J.-F., Bemer, E. & Hamon, Y. (2019) Effective medium modeling of diagenesis impact on the petroacoustic properties of carbonate rocks. *Geophysics*, 84(4), 43–57.

Anselmetti, F.S., Von Salk, G.A., Cunningham, K.J. & Eberli, G.P. (1997) Acoustic properties of Neogene carbonates and siliciclastics from the subsurface of the Florida Keys: implications for seismic reflectivity. *Marine Geology*, 144(1–3), 9–31.

Anselmetti, F.S. & Eberli, G.P. (2001) Sonic velocity in carbonates – a combined product of depositional lithology and diagenetic alterations. In: *Subsurface geology of a prograding carbonate platform margin, Great Bahama Bank: results of the Bahamas drilling project* (SEPM Special Publication 70). Tulsa: Society for Sedimentary Geology, pp. 193–216.

Bailly, C., Adelinet, M., Hamon, Y. & Fortin, J. (2019) Combined controls of sedimentology and diagenesis on seismic properties in lacustrine and palustrine carbonates (Upper Miocene, Samos Island, Greece). *Geophysical Journal International*, 219(2), 1300–1315.

Bailly, C., Fortin, J., Adelinet, M. & Hamon, Y. (2019) Upscaling of elastic properties in carbonates: a modeling approach based on a multiscale geophysical data set. *Journal of Geophysical Research, Solid Earth*, 124(12), 13021–13038.

Bailly, C., Kernif, T., Hamon, Y., Adelinet, M. & Fortin, J. (2022) Controlling factors of acoustic properties in continental carbonates: implications for high-resolution seismic imaging. *Marine and Petroleum Geology*, 137, 105518.

Berg, O.R. (1982) Seismic detection and evaluation of delta and turbidite sequences: their application to exploration for the subtle Trap1. *AAPG Bulletin*, 66(9), 1271–1288.

Beydoun, Z.R. (1977) Petroleum prospects of Lebanon: re-evaluation. *AAPG Bulletin*, 61(1), 43–64.

Boadu, F.K. & Long, L.T. (1996) Effects of fractures on seismic-wave velocity and attenuation. *Geophysical Journal International*, 127, 86–110.

Brew, G., Barazangi, M., Al-Maleh, A.K. & Sawaf, T. (2001) Tectonic and geologic evolution of Syria. *GeoArabia*, 6, 573–615.

Brown, A.B. (2001) Understanding seismic attributes. *Geophysics*, 66(1), 47–48.

Burberry, C.M., Jackson, C.A.-L. & Chandler, S.R. (2016) Seismic reflection imaging of karst in the Persian Gulf: implications for the characterization of carbonate reservoirs. *AAPG Bulletin*, 100, 1561–1584.

Chopra, S. & Marfurt, K.J. (2007) *Seismic attributes for prospect identification and reservoir characterisation*. Houston: Society of Exploration Geophysicists. ISBN 9781560801412.

Dercourt, J., Zonenshain, L.P., Ricou, L.-E., Kazmin, V.G., LePichon, X., Knipper, A.L. et al. (1986) Geological evolution of the Tethys

belt from the Atlantic to the Pamirs since the Lias. *Tectonophysics*, 123(1–4), 241–315.

Dix, C.H. (1955) Seismic velocities from surface measurements. *Geophysics*, 20, 68–86.

Dubertret, L. (1955) *Carte géologique du Liban au 1/200000*. Liban: Ministère des Travaux Publiques.

Dubertret, L. (1975) Introduction à la carte géologique au 1/50000 du Liban. *Notes et Mémoires sur le Moyen-Orient*, 23, 345–403.

Eberli, G.P., Baechle, G.T., Anselmetti, F.S. & Incze, M.L. (2003) Factors controlling elastic properties in carbonate sediments and rocks. *Leading Edge*, 22, 654–660.

Eberli, G.P., Masaferro, J.L. & Sarg, J.F. (2004) Seismic imaging of carbonate reservoirs and systems. *AAPG Memoir*, 81(81), 1–9.

Embry, J.-C., Hunt, D.W., Colpaert, A., Dræge, A. & Zahm, L. (2021) Seismic facies, stratigraphy, geomorphology, and seismic modelling of a Lower Cretaceous carbonate platform. *Geological Society, London, Special Publications*, 509(1), 89.

Emujakporue, G.O. & Enyenihi, E.E. (2020) Identification of seismic attributes for hydrocarbon prospecting of Akos field, Niger Delta, Nigeria. *SN Applied Sciences*, 2(5), 910.

Fontaine, J.M., Cussey, M., Lacaze, J., Lanaud, R. & Yapaudjian, L. (1987) Seismic interpretation of carbonate depositional environments. *AAPG Bulletin*, 71(3), 281–297.

Fournier, F. & Borgomano, J. (2007) Geological significance of seismic reflections and imaging of the reservoir architecture in the Malampaya gas field (Philippines). *AAPG Bulletin*, 91(2), 235–258.

Fournier, F., Leonide, P., Biscarrat, K., Gallois, A., Borgomano, J. & Foubert, A. (2011) Elastic properties of microporous cemented grainstones. *Geophysics*, 76(6), E211–E226.

Fournillon, A., Fournier, F. & Vidal, O. (2021) Seismic expression of carbonate build-up karstification: karst modelling strategies and insights from synthetic seismic. *Geological Society, London, Special Publications*, 509, 227–248.

Gardosh, M., Garfunkel, Z., Druckman, Y. & Buchbinder, B. (2010) Tethyan rifting in the Levant Region and its role in Early Mesozoic crustal evolution. *Geological Society, London, Special Publications*, 341(1), 9–36.

Garfunkel, Z. (1998) Constrains on the origin and history of the Eastern Mediterranean basin; collision-related processes in the Mediterranean region. *Tectonophysics*, 298, 5–35.

Ghoneimi, A., Farag, A.E., Bakry, A. & Nabih, M. (2021) A new deeper channel system predicted using seismic attributes in scarab gas field, west delta deep marine concession, Egypt. *Journal of African Earth Sciences*, 177, 104155.

Hawie, N., Deschamps, R., Nader, F.H., Gorini, C., Müller, C., Desmares, D. et al. (2013) Sedimentological and stratigraphic evolution of northern Lebanon since the Late Cretaceous: implications for the Levant margin and basin. *Arabian Journal of Geosciences*, 7(4), 1323–1349.

Hawie, N., Gorini, C., Deschamps, R., Nader, F.H., Montadert, L., Granjeon, D. et al. (2013) Tectono-stratigraphic evolution of the northern Levant Basin (offshore Lebanon). *Marine and Petroleum Geology*, 48, 392–410.

Hawie, N., Deschamps, R., Granjeon, D., Nader, F.H., Gorini, C., Müller, C. et al. (2015) Multi-scale constraints of sediment source to sink systems in frontier basins: a forward stratigraphic modelling case study of the Levant region. *Basin Research*, 29, 418–445.

Haq, B.U., Hardenbohl, J. & Vail, P.R. (1988) Mesozoic and Cenozoic chronostratigraphy and eustatic cycles. In: Wilgus, C.K., Hastings, B.J., Kendall, G.G., Posamentier, H., Ross, C.A. & Van Wagoner, J.C. (Eds.) *Sea-level changes: an integrated approach* (SEPM Special Publications, 42). Tulsa: SEPM, pp. 71–108.

Hendry, J., Burgess, P., Hunt, D., Janson, X. & Zampetti, V. (2021) Seismic characterisation of carbonate platforms and reservoirs. *Geological Society, London, Special Publications*, 509(1), SP509–2021–51.

Hossain, S. (2020) Application of seismic attribute analysis in fluvial seismic geomorphology. *Journal of Petroleum Exploration and Production Technology*, 10, 1009–1019.

Howell, J.A., Martinius, A.W. & Good, T.R. (2014) The application of outcrop analogues in geological modelling: a review, present status and future outlook. *Geological Society, London, Special Publications*, 387, 1–25.

Hu, X., Zheng, W., Zhao, X. & Niu, B. (2023) Quantitative characterization of deep fault-karst carbonate reservoirs: a case study of the Yuejin block in the Tahe oilfield. *Energy Geoscience*, 4(2), 100153.

Jafarian, E., De Jong, K., Kleipool, L.M., Scheibner, C., Blomeier, D.P.G. & Reijmer, J.J.G. (2018) Synthetic seismic model of a Permian biosiliceous carbonate – carbonate depositional system (Spitsbergen, Svalbard Archipelago). *Marine and Petroleum Geology*, 92, 78–93.

Kleipool, L.M., De Jong, K., De Vaal, E.L. & Reijmer, J.J.G. (2017) Seismic characterisation of switching platform geometries and dominant carbonate producers (Miocene, Las Negras, Spain). *Sedimentology*, 64, 1676–1707.

Lubbe, R. & Worthington, M.H. (2006) A field investigation of fracture compliance. *Geophysical Prospecting*, 54(3), 319–331.

Mangal, S., Hansa, G.L., Savanur, S.R., Roa, P.H. & Painuly, S.P. (2004) Identification of shallow gas prospect from DHC and inversion studies of 2D seismic data, Kosamba oil field, South Cambay Basin, Gujarat, India. In: *5th conference and exposition on petroleum geophysics, Hyderabad 4004, India*., Society of Exploration Geophysicists, pp. 782–787.

Matonti, C., Guglielmi, Y., Viseur, S., Bruna, P.O., Borgomano, J., Dahl, C. & Marié, L. (2015) Heterogeneities and diagenetic control on the spatial distribution of carbonate rocks acoustic properties at the outcrop scale. *Tectonophysics*, 638, 94–111.

McQuillin, R., Bacon, M. & Barclay, W. (1984) *An introduction to seismic interpretation: reflection seismic in petroleum exploration*, 2nd edition, London: Graham and Trotman Ltd.

Mitchum, R.M. (1977) Seismic stratigraphy and global changes of sea level, Part 1: Glossary of terms used in seismic stratigraphy. In: Payton, C.E. (Ed.) *Seismic stratigraphy—applications to hydrocarbon exploration*, vol. 26. Tulsa, Oklahoma: AAPG Memoir, pp. 205–212.

Nader, F.H. (2000) Petrographic and geochemical characterisation of the Jurassic–Cretaceous carbonate sequence of the Nahr Ibrahim Region (M.Sc. thesis). Lebanon: American University of Beirut.

Nader, F.H., Abdel-rahman, A.-F.M. & Haidar, A.T. (2006) Petrographic and chemical traits of Cenomanian platform carbonates (central Lebanon): implications for depositional environments. *Cretaceous Research*, 27, 689–706.

Nader, F.H., Swennen, R. & Ellam, R. (2007) Field geometry, petrography and geochemistry of a dolomitization front (Late Jurassic, central Lebanon). *Sedimentology*, 54(5), 1093–1119.

Nader, F.H. (2011) The petroleum prospectivity of Lebanon: an overview. *Journal of Petroleum Geology*, 34(2), 135–156.

Nader, F.H. (2014) *The geology of Lebanon*, Beaconsfield, UK: Scientific Press Ltd., 108 pp.

Nader, F.H., Browning-Stamp, P. & Lecomte, J.-C. (2016) Geological interpretation of 2D seismic reflection profiles onshore Lebanon: implications for petroleum exploration. *Journal of Petroleum Geology*, 39(4), 333–356.

Nanda, N.C. (2016) *Seismic data interpretation and evaluation for hydrocarbon exploration and production*. Berlin, Germany: Springer.

Noujaim, G. (1977) Pétrographie et environnements sédimentaires de l'Albien, Cénomanien, Turonien dans les environs Nord de Beyrouth (Liban) (PhD thesis). Paris, France: Université Pierre et Marie Curie.

Oyeyemi, K.D. & Aizebeokhai, A.P. (2015) Seismic attributes analysis for reservoir characterisation; offshore Niger delta. *Petroleum and Coal*, 57(6), 619–628.

Rekoske, K. & Hicks, D. (1992) Geophysical Methods. In: *Development geology reference manual*, vol. 10. AAPG, Tulsa, Oklahoma.

Robertson, A.H.F. (1998) Tectonic significance of the Eratosthenes Seamount: a continental fragment in the process of collision with a subduction zone in the eastern Mediterranean Ocean Drilling Program Leg 160. *Tectonophysics*, 298, 63–82.

Saint-Marc, P. (1972) Le Crétacé inférieur et moyen du bord occidental du Jabal-Sannine (Liban). *Notes et Mémoires sur le Moyen-Orient*, 13, 217–226.

Saint-Marc, P. (1974) Étude stratigraphique et micropaléontologique de l'Albien, du Cénomanien et du Turonien du Liban. *Notes et Mémoires sur le Moyen-Orient*, 13, 342.

Sayago, J., Di Lucia, M., Mutti, M., Cotti, A., Sitta, A., Broberg, K. et al. (2012) Characterization of a deeply buried paleokarst terrain in the Loppa High using core data and multiattribute seismic facies classification. *AAPG Bulletin*, 9(10), 1843–1866.

Sharland, P.R., Archer, R., Casey, D.M., Davies, R.B., Hall, S.H., Heward, A.P., Horbury, A.D. & Simmons, M.D. (2001) *Arabian plate sequence stratigraphy, GeoArabia* (GeoArabia Special Publication 2). Bahrain: Gulf Petrolink, p. 371.

Sheriff, R.E. (1977) Limitations on resolution of seismic reflections and geologic detail derivable from them. In: Payton, C.E. (Ed.) *Seismic stratigraphy—applications to hydrocarbon exploration*, vol. 26. Tulsa, Oklahoma: AAPG Memoir, pp. 3–14.

Słonka, Ł. & Krzywiec, P. (2020) Seismic characteristics and development of the upper Jurassic Carbonate Buildups from the Miechów Trough (Southern Poland). *Geosciences*, 10(6), 239.

Stafleu, J., Everts, A.J.W. & Kenter, J.A.M. (1994) Seismic models of a prograding carbonate platform: 1287 Vercors, south-east France. *Marine and Petroleum Geology*, 11(5), 514–527.

Stork, C. (2020) How does the thin near surface of the earth produce 10–100 times more noise on land seismic data than on marine data? *First Break*, 38(8), 67–75.

Teillet, T., Fournier, F., Borgomano, J. & Hong, F. (2020) Origin of seismic reflections in a carbonate gas field, Lower Miocene, offshore Myanmar. *Marine and Petroleum Geology*, 113, 104–110.

Vail, P.R., Mitchum, R.M. Jr. & Thomson, S. (1977) Seismic stratigraphy and global changes of sea level. In: Payton, C.E. (Ed.) *Seismic stratigraphy—applications to hydrocarbon exploration*, vol. 26. Tulsa, Oklahoma: AAPG Memoir, pp. 49–212.

Veeken, P. & Moerkerken, B. (2013) *Seismic stratigraphy and depositional facies models*, Houten, The Netherlands: EAGE Publications.

Wagner, P.D. (1997) Seismic signatures of carbonate diagenesis. In: Palaz, I. & Marfurt, K.J. (Eds.) *Carbonate seismology* (Geophysical Development Series, No. 6). Tulsa, Oklahoma: SEG, pp. 307–320.

Walley, C.D. (1997) The lithostratigraphy of Lebanon: a Review. *Lebanese Scientific Bulletin*, 10, 81–108.

Walley, C.D. (1998) Some outstanding issues in the geology of Lebanon and their importance in the tectonic evolution of the Levantine region. *Tectonophysics*, 298(1–3), 37–62.

Wang, Y. (2015) The Ricker wavelet and the Lambert W function. *Geophysical Journal International*, 200(1), 111–115.

Wood, B.G.M. (2015) Rethinking post-Hercynian basin development: eastern Mediterranean Region. *GeoArabia*, 20(3), 175–224.

Zeller, M., Reid, S.B., Eberli, G.P., Weger, R.J. & Massaferro, J.L. (2015) Sequence architecture and heterogeneities of a field-Scale Vaca Muerta analog (Neuquʹen Basin, Argentina) – from outcrop to synthetic seismic. *Marine and Petroleum Geology*, 66, 829–847.

How to cite this article: Abbani, G., Adelinet, M., Inati, L., Bailly, C. & Nader, F. (2023) Seismic characterization of Cenomanian–Turonian carbonate platform based on sedimentological and geophysical investigation of onshore analogue outcrop (northern Lebanon). *Geophysical Prospecting*, 71, 1616–1632. https://doi.org/10.1111/1365-2478.13396